Accurate and Efficient Modeling of Nucleation and Growth Processes

Scott T. Dunham, Iuval Clejan and Alp H. Gencer

Electrical and Computer Engineering Department,
Boston University, Boston, MA 02215.

Abstract

We have developed an efficient approach for modeling of nucleation and growth processes in nonhomogenous systems, by considering the evolution of the moments of the precipitate size distribution at each point on a spatial grid. Through the use of an energy-minimizing closure assumption, the size distribution can be reproduced from the moments, and thus the evolution of the moments can be derived directly from the full set of discrete rate equations describing the size evolution. The model has been implemented in a general reaction/diffusion simulator using a table look-up scheme for computational efficiency. We have tested the moment-based approach and found that it accurately reproduces the results of the full model over a range of processing conditions. The model has been applied with excellent results to processes occurring during VSLI fabrication (e.g., dopant precipitation, evolution of point defect clusters and dislocation loops following ion implantation), reproducing behavior such as Ostwald ripening and nucleation rates, as well as more complex phenomena such as reverse annealing and recovery following temperature steps. The modeling approach is general enough to apply to a large range of processes and materials systems and has been extended to consider the formation of aggregates with varying composition.

1 Introduction

Nucleation and growth processes play a critical role in a large range of materials processing systems. Because the behavior of precipitates is such a strong function of size, effective modeling of precipitation kinetics requires knowledge of the precipitate size distribution, which in turn depends on the thermal history of the sample. Classical modeling approaches divide such processes into two discrete steps, with nucleation and growth being modeled using fundamentally different assumptions, each valid only under idealized conditions. Thus, although these approaches are very useful for understanding qualitative behavior, they are unsuitable in many cases for the development of quantitative models, particularly under complex annealing conditions (e.g., multi-step anneals). Noting the power of modern computers to solve complex systems of coupled differential equations, we have developed a unified approach to modeling of nucleation and growth processes which extends nucleation theory to include the behavior of supercritical as well as subcritical precipitates. The parameters considered in the model are the change in energy with precipitate size and the reaction rate and solute diffusivity (for diffusive processes). By considering the evolution of the full size distribution over time, complex thermal history effects can be accurately modeled on a fundamental basis.

Many important material systems are nonhomogeneous due to initial and/or boundary conditions. Under such circumstances, solving for the evolution of the full precipitate distribution as well as solute diffusion/reaction at each spatial location can become computationally intractable, particularly for two or three-dimensional systems. To address this issue, we have developed a moment-based approach which leads to a reduction in the number of variables representing the precipitate distribution at each point in space from on the order of 100 or more to as few as 3, allowing us to reasonably incorporate it in a diffusion-reaction solver.

In this paper, we begin by describing the underlying model which considers to evolution of the full size distribution and give a couple of examples comparing this model to experimental observations of dopant precipitation in silicon. Next, we show how the precipitate size distribution can be described in terms of its moments and derive equations for the evolution of these moments. We compare the results of the moment-based modeling approach to the full model as well as to experimental observations of nucleation and growth kinetics in nonhomogenous systems arising during VLSI device fabrication. Next, we show how the moment-based approach can extended to multicomponent precipitation, and finally we summarize our conclusions.

2 Kinetic Equations for Evolution of Precipitate Size Distribution

The precipitation process is driven by the change in free energy with size. That energy can be written as the sum of a volume term which represents the change in energy upon adding a solute atom to an abitrarily large precipitate, plus the excess energy associated with finite size precipitates, including contributions from interface and strain energies:

$$\Delta G_n = -nkT \ln \left(\frac{C}{C^{ss}} \right) + \Delta G_n^{\mathrm{exc}}, \tag{1}$$

where n is the number of solute atoms, C is the solute concentration, and C^{ss} is the solid solubility. The form of $\Delta G_n^{\mathrm{exc}}$ depends on the system considered. In the simulations shown in this work, we assume it can be expressed as

$$\Delta G_n^{\mathrm{exc}} = c_1 n^{a_1} + c_2 n^{a_2} + \cdots \tag{2}$$

where $1 > a_1 > a_2 > \cdots$. The first term corresponds to the asymptotic behavior at large sizes, which is generally associated with the dependence of the active surface area on size (e.g., 2/3 for a sphere, 1/2 for a disk), and the other terms are corrections for the deviation of the free energy from this asymptotic behavior at small sizes.

Considering a precipitate that forms through the aggregation of solute atoms (perhaps in a compound with matrix atoms), the change in the concentration of precipitates of size n (f_n) is given by the difference between the net rates at which precipitates grow from size $n-1$ to n (I_{n-1}) and from size n to $n+1$ (I_n):

$$\frac{df_n}{dt} = I_{n-1} - I_n, \tag{3}$$

where $n \geq 2$. Since each growth step from n to $n+1$ involves a solute atom, the evolution of the solute concentration is given by

$$\frac{dC}{dt} = \nabla \cdot (D \nabla C) - 2I_1 - \sum_2^{\infty} I_n, \tag{4}$$

where D is the solute diffusivity and the factor of 2 for the I_1 is due to the fact that two solute atoms are required to make a cluster of size 2.

The net rate at which precipitates in the population grow from size n to $n+1$ is

$$I_n = g_n f_n - d_{n+1} f_{n+1}, \tag{5}$$

where g_n and d_n are the growth and dissolution rates, respectively, for a precipitate of size n. The exact form of the g_n and d_n depend on the growth mechanism and the diffusion field around each precipitate [1, 2]. Assuming spherical precipitates, first order growth kinetics, diffusion fields around each precipitate as would exist under quasi-steady state conditions (constant growth rate

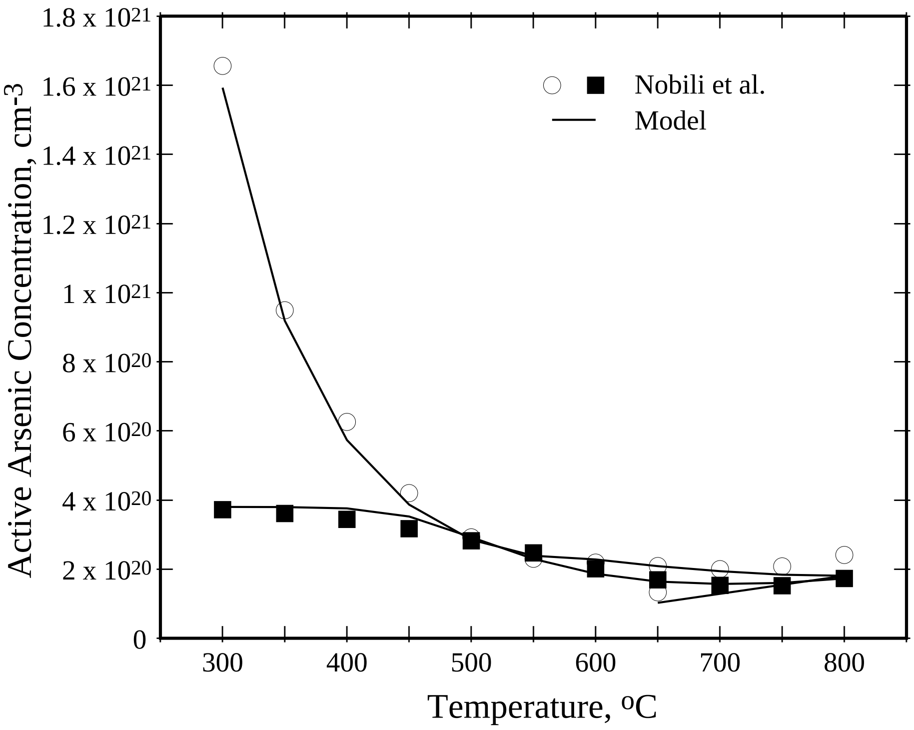

Figure 1: *Measured and simulated active arsenic doping levels for two different initial arsenic concentrations at each stage of a series of 1 h anneals at 50°C intervals starting at 300°C. After the final 800°C anneal, the samples were annealed for an additional 100 h at 650°C. The samples were initially fully activated via a laser anneal. Data from Nobili et al. [3].*

and interface and bulk solute concentrations), and a solute concentration in the matrix much smaller than that in the precipitate phase,

$$g_n = \frac{DA_nC}{R_n + \lambda}, \quad d_{n+1} = \frac{DA_nC_n^*}{R_n + \lambda}, \tag{6}$$

where A_n is the surface area of a precipitate with n solute atoms, R_n is its radius, $\lambda = D/k_n$, k_n is the interface reaction rate. C_n^* is the concentration of solute atoms for which there is no change in the system energy for a precipitate growing from size n to $n+1$ ($g_n = d_{n+1}$):

$$C_n^* = C \exp\left(\frac{\Delta G_{n+1} - \Delta G_n}{kT}\right) = C^{ss} \exp\left(\frac{\Delta G_{n+1}^{\mathrm{exc}} - \Delta G_n^{\mathrm{exc}}}{kT}\right) \tag{7}$$

We have applied this system based on discrete rate equations (Eq. 3) to the modeling of dopant precipitation in silicon during multi-step annealing cycles with excellent results [1, 2]. Figures 1 and 2 show examples of comparisons of the model to measurements of the evolution of electrically active arsenic concentration (solute concentration) during annealing of laser annealed samples as reported by Nobili *et al.* [3]. Note that the laser annealing caused melting of the sample surface, resulting in full activation (dissolution) of the arsenic as well as a uniform concentration profile up to the melt depth. The low arsenic diffusivity at annealing temperatures below 800°C led to negligible spreading of the arsenic profile, so that the system could be considered equivalent to bulk precipitation in a homogeneous system and only a single size distribution was simulated. The behavior shown in Figure 2 illustrates the importance of considering the full size distribution in predicting precipitation behavior. Despite the fact that the solute concentration remains well above the solubility at 750°C

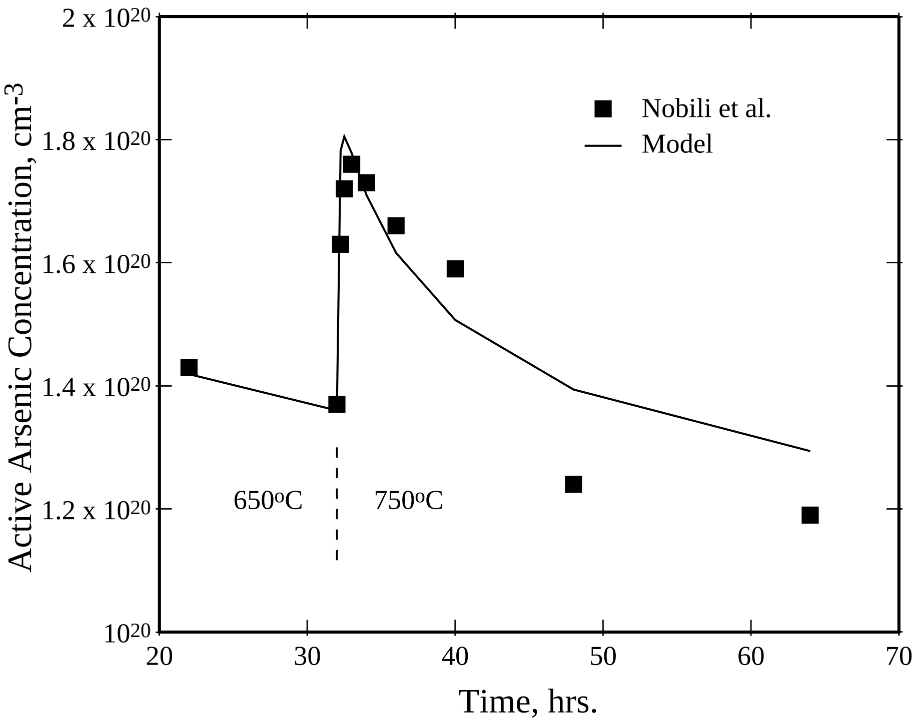

Figure 2: *Measured and simulated active arsenic doping levels for annealing of a fully-activated laser-annealed sample ($C(t = 0) = 1.5 \times 10^{21}\mathrm{cm}^{-3}$) for 32 h at 650°C, followed by additional annealing at 750°C. Data from Nobili et al. [3].*

($C^{ss} = 1.1 \times 10^{20}$), reverse annealing (e.g., net precipitate dissolution) is initially observed following the rise in annealing temperature. The reason for this behavior is illustrated in Fig. 3, which shows the simulated size distribution just before and 15 min after the temperature increase. The higher temperature results in an increase in the solubility and thus the critical size. Initially the population of precipitates below the new critical size are present at concentrations higher than the quasi-equilibrium distribution associated with the solute concentration, and thus they rapidly shrink and dissolve leading to the observed reverse annealing. Once a new quasi-equilibrium distribution of subcritical precipitates is established, the precipitation process continues through nucleation and growth.

3 Reduced Moment-Based Model

The model described in the previous section is very effective in simulating nucleation and growth processes, but it is computationally expensive for nonhomogeneous systems in which the full size distribution would need to be tracked at each point in space. In order to develop a more efficient approach, we describe the size distribution in terms of a small number of moments and consider only the evolution those moments rather than the full distribution at each point in space. The moments are defined as:

$$m_i = \sum_{2}^{\infty} n^i f_n. \tag{8}$$

The zeroth order moment of the distribution is simply the precipitate density, while the first moment corresponds to the density of precipitated solute atoms. Higher order moments further describe the shape of the size distribution.

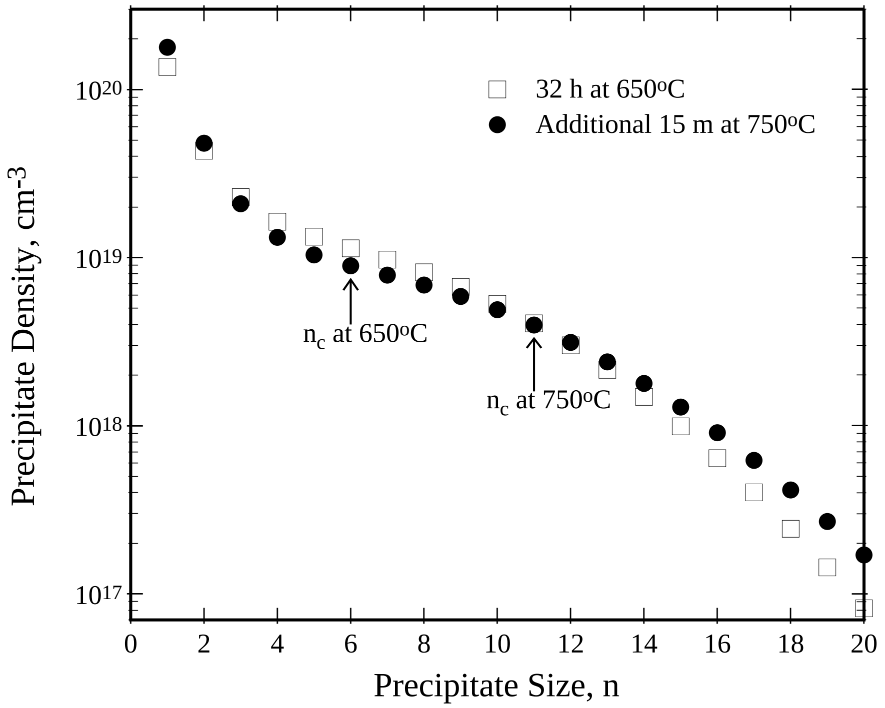

Figure 3: *Simulated precipitate size distributions after a 32 h at 650*°C *and after an additional 15 min at 750*°C*. Also indicated are the critical precipitate size before (*$n_c(650°\mathrm{C}) = 6$*) and after (*$n_c(750°\mathrm{C}) = 11$*) the temperature step.*

Since any finite number of moments is insufficient to describe an arbitrary distribution, it is necessary to add a closure assumption. We assume that the precipitate size distribution is the one that minimizes the Gibbs free energy, constrained such that the population of precipitates has the known values of the simulated moments. Applying our closure assumption and minimizing the free energy, considering moments 0 through I are used, the resulting distribution is

$$f_n = \exp\left(-\frac{\Delta G_n^{\mathrm{exc}}}{kT} + \sum_{i=0}^{I} \xi_i n^i\right), \tag{9}$$

where the ξ_i are the Lagrange multipliers from the constrained minimization. The values of the ξ_i can be determined by substituting Eq. 9 into Eq. 8 and solving. Thus, the assumed distribution f_n depends only on $\Delta G_n^{\mathrm{exc}}$, the temperature and the moments m_0 through m_I, and is independent of the solute concentration.

To determine the time evolution of the moments, we simply differentiate Eq. 8 and substitute in the expression for the evolution of f_n from the discrete rate equation formulation (Eq. 3):

$$\frac{dm_i}{dt} = \sum_{2}^{\infty} n^i (I_{n-1} - I_n). \tag{10}$$

The evolution of the first few moments is thus:

$$\frac{dm_0}{dt} = g_1 C^2 - d_2 f_2 = I_1 \tag{11}$$

$$\frac{dm_1}{dt} = 2I_1 + \sum_{2}^{\infty} (g_n f_n C - d_{n+1} f_{n+1}) \tag{12}$$

$$\frac{dm_2}{dt} = 4I_1 + \sum_2^\infty (2n+1)(g_n f_n C - d_{n+1} f_{n+1}) \qquad (13)$$

Similarly, the evolution of the solute density is just

$$\frac{dC}{dt} = \nabla \cdot (D \nabla C) - \frac{dm_1}{dt} = \nabla \cdot (D \nabla C) - 2I_1 - \sum_2^\infty (g_n f_n C - d_{n+1} f_{n+1}) \qquad (14)$$

As noted above, f_n can be calculated from the moments. However, this process requires solving a set of transcendental equations. Because these sums do not depend on the doping density (any dependence of the diffusivity on concentration can be factored out), instead of solving these equations numerically at each time step, we precompute tables of values for the sums on the right hand side of Eqs. 13–11 and interpolate from the tables during simulations [4, 5]. These tables have dimension I rather than $I + 1$ since f_n scales linearly with the number of precipitates (m_0). The tables thus give values of the sums over f_n/m_0 as functions of m_i/m_0 ($1 \leq i \leq I$).

We have implemented this moment-based approach for precipitation kinetics in DOPDEES [6], a process simulator with the ability to solve arbitrary sets of partial differential equations in one dimension using an object-oriented approach to operator definition which simplifies the development of new models. We are thus able to simulate precipitation behavior in nonhomogeneous systems, as well as to include precipitation as one of many processes occuring in complex multicomponent systems such as those present during integrated circuit fabrication. As described in the next section, the moment-based approach gives excellent agreement with both experimental observations as well as with results of the full model on which it is based.

4 Comparison of Reduced Model to Full Model and Experiment

The ability of the reduced model to match the evolution of the full precipitate size distribution using only a small number a moments relies on how accurately the distribution as given by these moments in conjunction with our closure assumption matches the actual distribution. We find that the closure assumption does in fact do an excellent job of reproducing the full distribution from only the lowest three moments (m_0, m_1 and m_2).

As a test of our approach, we ran simulations of arsenic and phosphorus precipitation using the full set of discrete rate equations for a variety of time and temperature schedules and initial solute levels. We then extracted the moments of the resulting precipitate distributions, and from those moments constructed the distributions assumed by the moment-based approach. Figure 4 shows an example of that comparison for what should be one of the most difficult conditions to match: the reverse annealing regime illustrated in Fig. 2. As can be seen, although the profile shapes are very distinctive and clearly non-Gaussian, the two distributions are almost identical, demonstrating the effectiveness of minimizing the free energy of the distribution as a closure assumption. We find similar agreement for other annealing conditions of interest, although for very long aging times, additional constraints are necessary in order to accurately reproduce the distribution. One reason for the excellent agreement is that the minimization of free energy leads to a density of subcritical precipitates that closely approximates the quasi-equilibrium distribution for the given current solute concentration. This occurs even though, once the moments are given, the distribution is independent of the solute concentration, because the rapid response of the smaller precipitates to changes in solute concentration is reflected in the evolution of the moments.

In order to compare the moment-based approach to experimental measurements, as well as the full model on which it is based, we use model parameters calculated by applying the full model to arsenic and phosphorus activation/deactivation behavior at temperatures below 800°C. Note

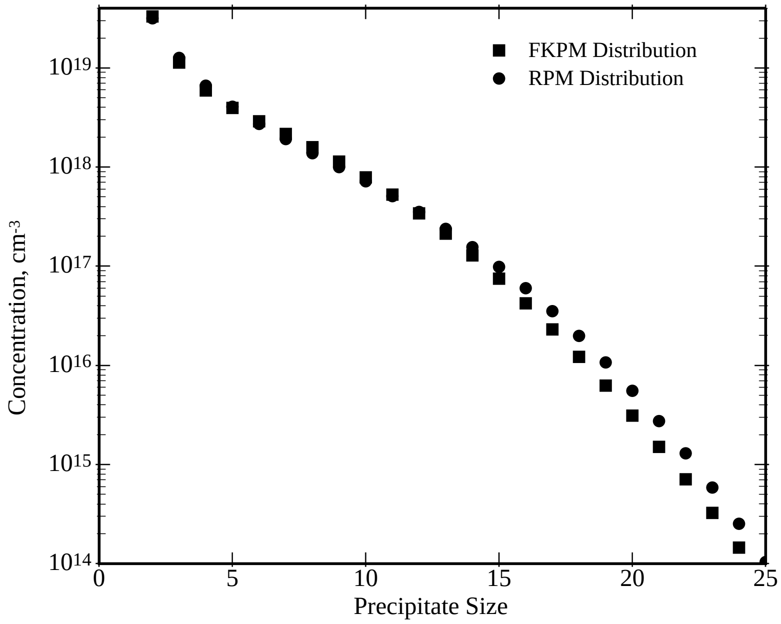

Figure 4: *Comparison of precipitate size distribution from solution of discrete rate equations to profile with the same zeroth, first and second moments calculated using the closure assumption of the moment-based approach. Simulations were for an initial fully-activated (laser-annealed) arsenic concentration of* $1.5 \times 10^{21}\mathrm{cm}^{-3}$ *and an annealing schedule consisting of 32 h at 650*°C *followed by an additional 15 min at 750*°C.

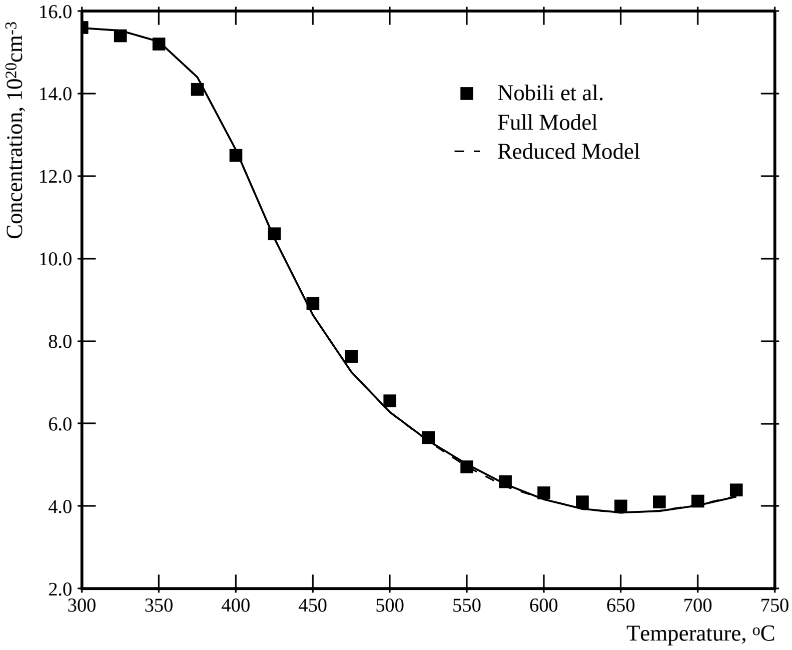

Figure 5: *Peak active phosphorus concentration following each step of a series of one hour anneals. The sample was initially implanted and laser annealed resulting in a box-like profile. The reduced model is nearly indistinguishable from steady state model. Data from Nobili et al. [7].*

that the two models share parameters as well as basic model assumptions, with the moment-based approach differing only in that the distribution is described by its lowest moments, rather than being given explicitly. Because of this direct correspondence, it is straightforward to incorporate any modifications in the full model directly into the reduced model.

In Figure 5, the two models are compared with data for active doping level (solute concentration) in a heavily phosphorus-doped and laser-annealed wafer annealed for 1 h at each of a series of temperatures from 300 to 725°C. For these conditions, the moment-based approach almost exactly reproduces the full model and both models match the experimental data closely. In Figure 6, we show a comparison of phosphorus activation data from a two-step annealing experiment by Nobili *et al.* [7], similar to that shown in Fig. 2, with both of the modeling approaches. Again, the reduced model gives very similar results to the full model, even immediately following the temperature transient.

Because of its computational efficiency, we can apply the moment-based approach using the same model and parameters at higher temperatures where substantial diffusional broadening of the profile occurs by evolving the precipitate distribution at each point on a spatial grid. In Figure 7, we compare the results of a simulation of an 8 min anneal of a laser annealed arsenic profile at 1000°C with the measured chemical profile [8]. As can be seen, the simulation does an excellent job of matching the precipitation behavior and the profile shape.

In addition to dopant precipitation, we have also applied the moment-based approach to the aggregation of silicon interstitials into {311} planar defects and dislocation loops following the implantation of silicon ions into silicon [9, 10, 11]. The system is highly nonhomogeneous since in addition to the initial non-uniform interstitial profile from the implant, interstitials diffuse rapidly to segregate and/or regrow at the wafer surface. Figure 8 shows the evolution of the total number

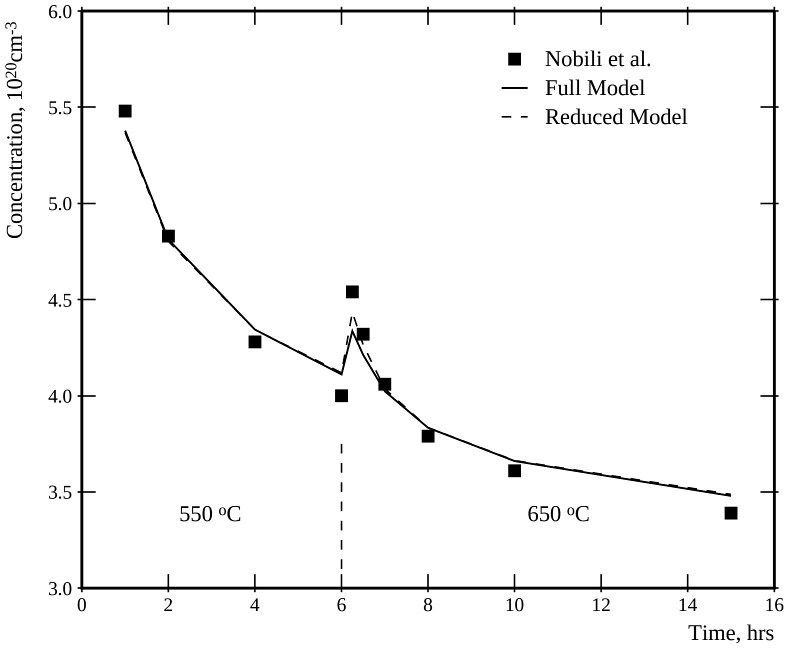

Figure 6: *Peak active phosphorus concentration for two-step anneal. Initial sample is implanted and laser annealed. The temperature is annealed first at 550°*C *for 6h and then the temperature is changed to 650°*C*. Data from Nobili Nobili et al. [7].*

of interstitials in {311} defects (m_1 integrated over depth) and the average size of those defects (m_1/m_0) for annealing of a $5 \times 10^{13}\,\mathrm{cm}^{-2}$, $40\,\mathrm{keV}$, Si implant at various temperatures. The experimental values are based on plan view and high resolution cross-sectional TEM observations by Eaglesham *et al.* [12]. The model does a very good job of matching the loss of interstitials to the surface as well as the ripening of the precipitate population. These two processes are interlinked as the flux to the surface depends on the concentration of interstitials (solute atoms) in the neighborhood of the defects, which drops as the average defect size increases. Figure 9 shows the simulated depth distribution of the total excess interstitial concentration ($C_I + m_1$) which shows that the population of {311} defects erodes from both sides as interstitials diffuse towards the surface and into the bulk. (Note that the interstitial concentration varies approximately linearly between the region containing extended defects and the surface, although it shows up as strongly curved in Fig 9 due to the logarithmic vertical scale.) It is the combination of the reduction in C_n^* due to the ripening of the defect population, the shifting of the upper edge of the extended defect distribution deeper into the substrate, and interface segregation behavior that together give the almost exponential (rather than linear) decay in the total interstitial concentration observed.

5 Precipitation of Compound Phases

In the models described above, we have considered the precipitation of a single solute species in either an elemental phase or as a compound with matrix atoms. However, in many systems, multiple solutes aggregate together to form compound phases. Focusing on a two-solute system for simplicity (e.g., $\mathrm{A}_n\mathrm{B}_m$), there are several choices for modeling such processes within the moment-based framework. The most general approach considers arbitrary precipitate compositions which

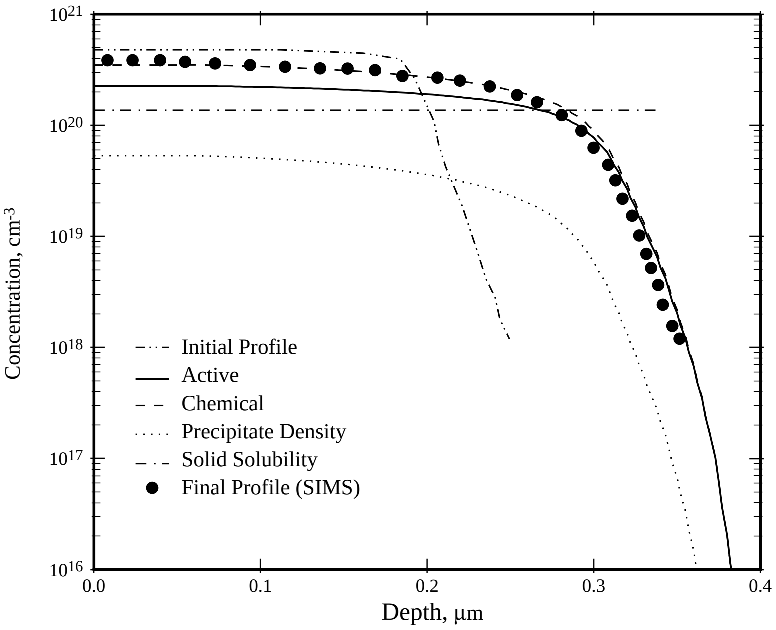

Figure 7: *Active and total (chemical) arsenic concentration profiles after an 8 minute RTA at 1000°C based on simulation of simultaneous diffusion and precipitation. Also shown is the precipitate density and the solid solubility. Initial and final experimental profiles are from Rousseau et al. [8]. Simulated profiles were convolved with the calculated SIMS response.*

evolve in a multi-dimensional size space ($f_{n,m}$ for a two solute species). For such a system, direct solution of the full set of discrete rate equations becomes computationally expensive even if the system can be considered homogeneous. However, extension of the moment-based approach is straightforward. It is necessary to add at least one moment to the system to represent the evolution in m,

$$m_m = \sum_{n,m} m f_{n,m}, \tag{15}$$

and the other moments are similarly summed over both n and m. The precipitate free energy becomes a function of both solute concentrations and the precipitate composition, as well as size:

$$\Delta G_{n,m} = -nkT \ln\left(\frac{C_A}{C_A^{ss}}\right) - mkT \ln\left(\frac{C_B}{C_B^{ss}}\right) + \Delta G_{n,m}^{\text{exc}}, \tag{16}$$

Using the energy minimizing closure assumption, the distribution given the moments m_0, m_1, m_2 and m_m is

$$f_{n,m} = K \exp\left(-\frac{\Delta G_{n,m}^{\text{exc}}}{kT} + \xi_1 n + \xi_2 n^2 + \xi_m m\right), \tag{17}$$

where $K = \exp(\xi_0)$). The correlations between n and m are handled naturally by the $\Delta G_{n,m}^{\text{exc}}$ term, and the equations for the evolution of the moments can be easily derived as described in Section 4.

For some systems, the precipitate composition will be fixed (e.g., $m = \gamma n$), which leads to a simplification of the above system. The concentration of solute B can then be considered to modify the effective solubility of solute A (or vice-versa),

$$\Delta G_n = -nkT \ln\left[\left(\frac{C_A}{C_A^{ss}}\right)\left(\frac{C_B}{C_B^{ss}}\right)^{\gamma}\right] + \Delta G_n^{\text{exc}}. \tag{18}$$

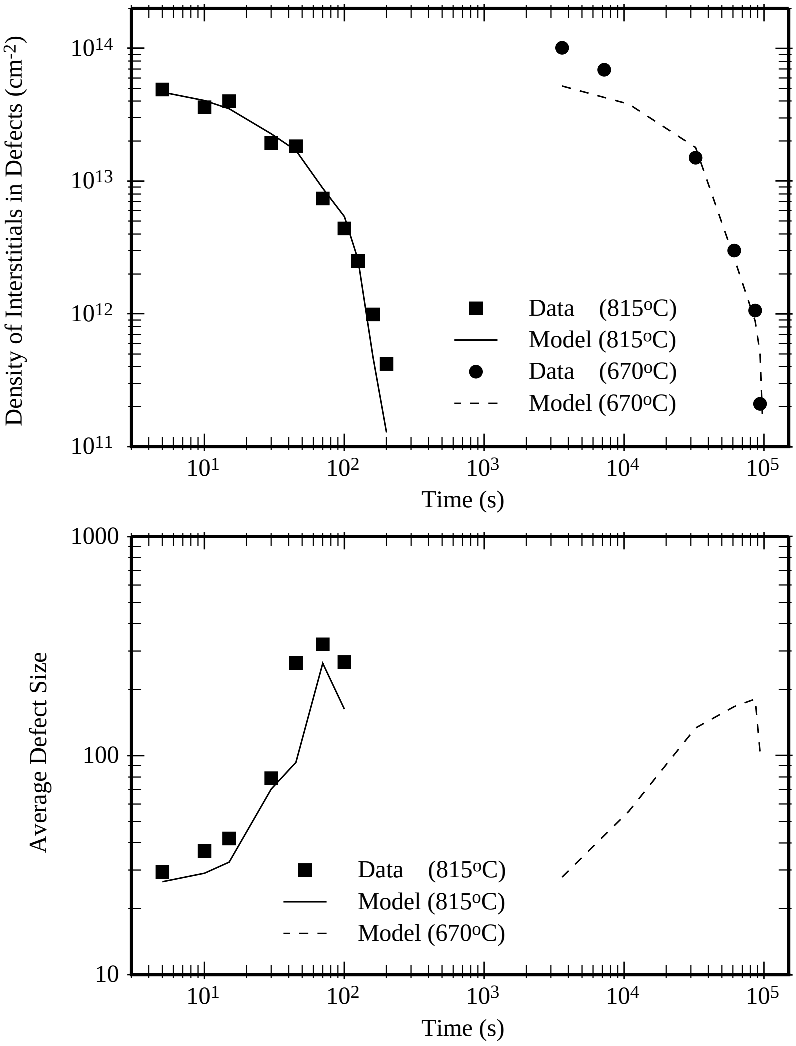

Figure 8: *Comparison between simulation and experiment for time evolution of (a) areal density of interstitials in {311} defects (m_1 integrated over depth) and (b) average defect size (m_1/m_0) for 815°C and 670°C anneals of a $5 \times 10^{13}\mathrm{cm}^{-2}$, 40 keV, Si implant into Si. Data from Eaglesham et al. [12].*

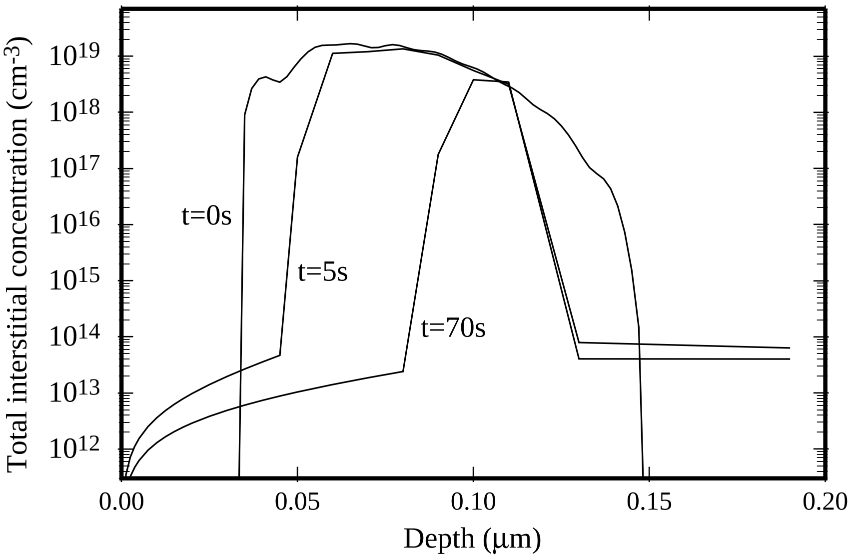

Figure 9: *Simulated total concentration of excess silicon atoms (both aggregated and free interstitials) versus depth after 0, 5 and 70 s 815*°C *anneals of* a $5 \times 10^{13}\mathrm{cm}^{-2}$, *40 keV, Si implant into Si.*

and the growth/dissolution kinetics modified to include limitations on the rates imposed by the diffusion and incorporation of both species [13]. However, given these changes in the full model, the derivation of the moment evolution remains as described in Section 4.

We have actually implemented an intermediate approach, which considers the fact that as the ratio of the solute species changes, the composition of the precipitating phase can be expected to change as well. We have applied this approach in modeling the incorporation of point defects (interstitials and vacancies) in the precipitation of boron and arsenic in silicon (e.g., $\mathrm{B}_n\mathrm{I}_m$ and $\mathrm{As}_n\mathrm{V}_m$) [14, 15]. Defining an excess energy which depends on both n and m ($\Delta G^{\mathrm{exc}}_{n,m}$), we assume that interactions with point defects are rapid such that for each value of n, the value of m is chosen to minimize the free energy for the given point defect concentration. Thus, only the moments of the distribution over n are required as solution variables, but $\gamma(n)$ increases as the concentration of the incorporated point defect increases. Figure 5 shows an example of the application of this model to the simulation of diffusion and precipitation of a boron delta-doped superlattice in a silicon substrate following silicon implantation. The implanted silicon causes an interstitial supersaturation which in turn leads to both immobile peaks in the boron profiles from to the reduction in the effective solid solubility Eq. 18, as well as enhanced diffusion via an interstitial mechanism of the remaining dissolved boron (negligible profile broadening would be expected under equilibrium conditions). We have also applied the same approach to $\mathrm{As}_n\mathrm{V}_m$ co-precipitation [14, 15], with excellent match to both the precipitation kinetics as well as the changes in point defect concentrations (vacancy undersaturation and corresponding interstitial supersaturation via Frenkel pair recombination) as measured by the use of a boron marker layer [16].

6 Conclusions

We have developed a unified model for nucleation and growth processes involving the solution of a series of discrete rate equations. We have found the approach to be particularly useful in modeling of complex annealing schedules which are difficult to deal with using classical approaches. For efficient simulation of precipitation processes, particularly in nonhomogeneous systems, we

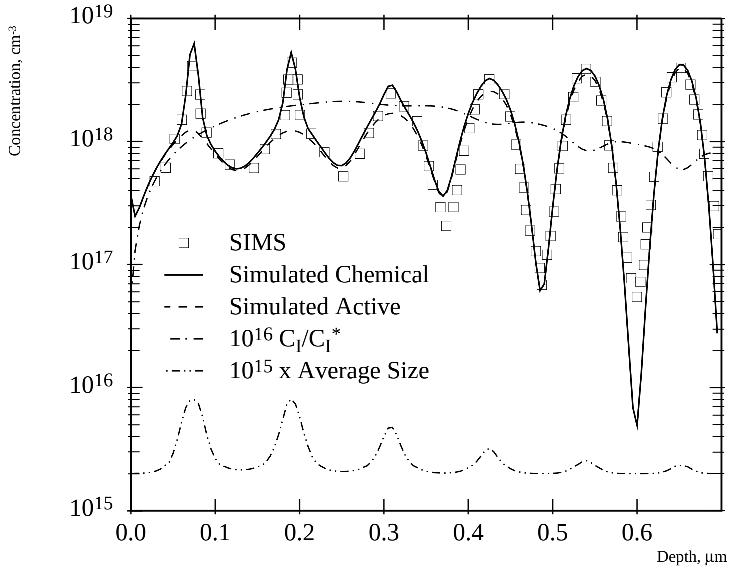

Figure 10: *Simulated total and active boron doping, interstitial concentration and average cluster size for a boron delta-doped superlattice implanted with* $5 \times 10^{13}\mathrm{cm}^{-2}$ *40 keV Si and annealed for 10 min at 790°*C. *The initial profiles had a standard deviation on the order of 0.005*μm. *Data from Stolk et al. [17].*

have developed a reduced, moment-based model which can be derived directly from the full set of discrete rate equations using an energy-minimizing closure assumption. We have successfully implemented the model in a general one-dimensional diffusion simulator and applied it to dopant activation/deactivation and interstitial aggregation in silicon. The model agrees well with experimental observations and is able to duplicate the results of the full set of discrete rate equations, while greatly reducing the number of variables required, with a corresponding reduction in the computational resources required.

Because the approach described in this work provides a framework for direct derivation of reduced moment-based models from models which explicitly consider the full size distribution, it is straightforward to apply the technique to other problems or to modify the assumptions made to consider for example, different dependences of precipitate energy on size or alternative growth mechanisms. In addition, the implementation in a general PDE solver of the model, along with table generation and look-up for efficient simulation, make it easy to apply to new applications involving multiple diffusing, reacting, and precipitating species. We have shown that it is possible to extend the approach to consider the precipitation of compound phases and multiple solute species, and have demonstrated the effectiveness of the approach for modeling point defect incorporation in dopant precipitates in silicon.

Acknowledgements

This work was supported by the Semiconductor Research Corporation and SEMATECH.

REFERENCES

[1] S. T. Dunham, in **Semiconductor Silicon**, eds. H. R. Huff, W. Bergholz and K. Sumino (Electrochemical Society Proc. **94-10**, 1994) p. 711.

[2] S. T. Dunham, *J. Electrochem. Soc.* **142**, 2823 (1995).

[3] D. Nobili, A. Carabelas, G. Celotti and S. Solmi, *J. Electrochem. Soc.* **130**, 922 (1983).

[4] I. Clejan and S. T. Dunham, in **ULSI Science and Technology**, E.M. Middlesworth and H.Z. Massoud, eds. (Electrochem. Soc. Proc., Pennington, NJ, 1995).

[5] I. Clejan and S. T. Dunham, *J. Appl. Phys.* **78**, 7327 (1995).

[6] A.H. Gencer, *DOPDEES User's Manual* (1996).

[7] D. Nobili, A. Armigliato, M. Finetti and S. Solmi, *J. Appl. Phys.* **53**, 1484 (1982).

[8] P. M. Rousseau, P. B. Griffin, P. G. Carey and J. D. Plummer, in **Process Physics and Modeling**, G. R. Srinivasan, K. Taniguchi and C. S. Murthy, eds. (Electrochem. Soc. Proc. **93-6**, Pennington, NJ, 1993) p. 130.

[9] A. H. Gencer and S. T. Dunham, in Process Physics and Modeling in Semiconductor Technology, G. R. Srinivasan, C. S. Murthy and S. T. Dunham, eds. (Electrochem. Soc. Proc., Pennington, NJ 1996).

[10] A. H. Gencer and S. T. Dunham, *J. Appl. Phys.* (1997). (in press)

[11] A. H. Gencer and S. T. Dunham, in **Microstructure Evolution During Irradiation**, T. de la Rubia, L. Hobbs, I. Robertson and G. Was, eds. (Mat. Res. Soc. Proc. 439, Pittsburgh, PA, 1997); also in **Materials Modification and Synthesis by Ion Beam Processing**, D. Alexander, N. Cheung, B. Park and W. Skorupa, eds. (Mat. Res. Soc. Proc. 439, Pittsburgh, PA, 1997).

[12] D. J. Eaglesham, P. A. Stolk, H. J. Gossmann, and J. M. Poate, *Appl. Phys. Lett.* **65**, 2305 (1994).

[13] W. A. Tiller and S. Oh, *J. Appl. Phys.* **64**, 375 (1988).

[14] I. Clejan and S. T. Dunham, in **Process Physics and Modeling in Semiconductor Technology**, G.R. Srinivasan, C.S. Murthy and S. T. Dunham, eds. (Electrochem. Soc. Proc., Pennington, NJ 1996).

[15] I. Clejan and S. T. Dunham, *J. Appl. Phys.* (in review)

[16] P. M. Rousseau, P. M. Griffin and J. D. Plummer *IEDM Tech. Dig.* (1994).

[17] P. A. Stolk, H. J. Gossmann, D. J. Eaglesham, and J. M. Poate, *Nucl. Instr. and Meth. in Phys. Res.* **B 96**, 187 (1995).